



HAL
open science

Synthesis, structure, photophysical properties and biological activity of a cobalt(II) coordination complex with 4,4'-bipyridine and porphyrin chelating ligands

N. Amiri, S. Nour, M. Hajji, T. Roisnel, T. Guerfel, G. Simonneaux, H. Nasri

► To cite this version:

N. Amiri, S. Nour, M. Hajji, T. Roisnel, T. Guerfel, et al.. Synthesis, structure, photophysical properties and biological activity of a cobalt(II) coordination complex with 4,4'-bipyridine and porphyrin chelating ligands. *Journal of Saudi Chemical Society*, 2019, 23 (7), pp.781-794. 10.1016/j.jscs.2019.03.003 . hal-02122167

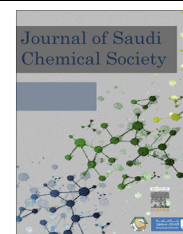
HAL Id: hal-02122167

<https://univ-rennes.hal.science/hal-02122167>

Submitted on 9 Jul 2020

HAL is a multi-disciplinary open access archive for the deposit and dissemination of scientific research documents, whether they are published or not. The documents may come from teaching and research institutions in France or abroad, or from public or private research centers.

L'archive ouverte pluridisciplinaire **HAL**, est destinée au dépôt et à la diffusion de documents scientifiques de niveau recherche, publiés ou non, émanant des établissements d'enseignement et de recherche français ou étrangers, des laboratoires publics ou privés.



ORIGINAL ARTICLE

Synthesis, structure, photophysical properties and biological activity of a cobalt(II) coordination complex with 4,4'-bipyridine and porphyrin chelating ligands



Nesrine Amiri^a, Sahar Nouir^b, Melek Hajji^{c,*}, Thierry Roisnel^d, Taha Guerfel^c, Gérard Simonneaux^d, Habib Nasri^a

^a Laboratory of Physico-Chemistry of Materials, University of Monastir, Avenue of the Environment, 5019 Monastir, Tunisia

^b Laboratory of Biochemistry, Faculty of Medicine, University of Sousse, Tunisia

^c Research Unit: Electrochemistry, Materials and Environment, University of Kairouan, 3100 Kairouan, Tunisia

^d Institute of Chemical Sciences of Rennes, UMR 6226, University of Rennes 1, Beaulieu Campus, 35042 Rennes, France

Received 4 January 2019; revised 14 March 2019; accepted 17 March 2019

Available online 23 March 2019

KEYWORDS

Cobalt(II)-porphyrin framework;
X-ray crystallography;
DFT;
Optical spectroscopies;
Antioxidant activity

Abstract A new bioactive material of cobalt(II) with 5,10,15,20-tetrakis[4 (benzoyloxy)phenyl] porphyrin (TPBP) and bpy ligands ($[\text{Co}^{\text{II}}(\text{TPBP})(\text{bpy})_2]$ **1**) has been synthesized and characterized by Single-crystal X-ray diffraction (SCXRD), spectroscopic methods and quantum-chemistry calculations. In the crystalline structures of six coordinated Co(II) $[\text{Co}^{\text{II}}(\text{TPBP})(\text{bpy})_2]$ **1**, linear 1D polymeric chains were observed in which all the porphyrin units are aligned parallel to each other. The crystal packing is stabilized by inter- and intramolecular C–H···O and C–H···N hydrogen bonds, and by weak C–H···Cg π interactions. Interestingly, NBO–Second-order perturbation theory analysis, carried out at the UB3LYP/6-31G(d)/SDD DFT level of theory, demonstrated that a two-center bond between the nitrogen atoms and the cobalt ions (Co) was not found, the Co–N_{py/bp} interactions are coming from an electronic delocalization between the N_{py/Nbp} filled orbitals to the anti-bonding LP*(4) and LP*(5) metal NBOs. Mass spectroscopy, and elemental analysis were also investigated to confirm the molecular structure. The downfield shift and the peak broadening of the axial ligand resonances observed in the ¹H NMR indicated the contiguity to the paramagnetic Co(II) center. Additionally, the photophysical properties have been evaluated by UV–visible

* Corresponding author.

E-mail address: melekhajji.univk@gmail.com (M. Hajji).

Peer review under responsibility of King Saud University.



Production and hosting by Elsevier

absorption, and fluorescence emission spectroscopies. Finally, bioactivity investigations revealed that free porphyrin TPBP, Co^{II}TPBP and complex **1** could be used as potential antioxidant agents. © 2019 King Saud University. Production and hosting by Elsevier B.V. This is an open access article under the CC BY-NC-ND license (<http://creativecommons.org/licenses/by-nc-nd/4.0/>).

1. Introduction

Porphyrin-containing metal complexes have received much interest due to their structural diversity and wide applications in gas storage, compound separation, chemical sensing and heterogeneous catalysts [1–4]. Owing to conjugated configuration, porphyrin and metalloporphyrin units are remarkable precursors in supramolecular chemistry as excellent components in the design of efficient molecular materials with improved electrochemical and photo-physical properties [5]. Indeed, they are engaged in several projects, including molecular wires [6], chemical sensors [7], semi-conductors [8], photo-induced electron transfer [9,10], and solar photovoltaic cells [11]. One interesting application of metalloporphyrins is found in catalysis, where the metal center is used as an active site [12]. In addition, recent in vitro studies demonstrated that porphyrins are also effective against viruses and yeasts [13,14]. That is, the porphyrinic nucleus presents an efficient source for the synthesis of a large number of antimicrobial and antioxidant active agents [15–17]. In addition, several derivatives of porphyrin have been developed as photosensibilizing agents (PS) for photodynamic therapy (PDT) [18–20]. Over the last few decades, many crystalline structures of porphyrins or metalloporphyrins have been reported whose optical properties and crystal packing are governed by axial ligand coordination modes [21]. Among the M(II)-porphyrins, the cobalt(II) porphyrins are most intensively studied compounds, since they are more sensitive to light irradiation and have the ability to change their oxidation state. [22]. Central cobalt atom in porphyrin frameworks can be bonded to one apical or two axial ligands, as the coordination by one ligand yields monomer and dimer assemblies, whereas coordination by two ligands gives monomers and polymeric structures. Supramolecular monomer complexes were obtained for cobalt(II) porphyrins with monodentate ligands such as imidazole, dimethylaminopyridine, pyridine and piperidine [23–26]. Cobalt(II) metalloporphyrins with bidentate bpy are generally existing as polymer species [Co^{II}(Porph)(bpy)₂]_n [27–29], and dimers [Co(Porph)₂(bpy)] [30]. As reported in the literature, 1D coordination polymers [24,25] have been prepared whose interlayer distance between porphyrin networks is controlled by a suitable bidentate spacer bpy ligand, bridging adjacent metalloporphyrin cores along the axial direction. Dey and co-workers [31], described a one-dimensional polymers ([Co^{II}(tn-OEP)(L)]_n) with different types of ligands: 4,4'-diazene-1,2-diyl dipyridine or 4-((pyridin-4-yl)methylene)carbohydrazonoylpyridine based on tetranitrooctaethylporphyrin (tn-OEP). These complexes are emerging as candidates in Photoelectrochemical and Photocatalysis Measurements [32]. In addition, our research group have a large experience on the design and characterization of new metalloporphyrin-based materials, in which bpy ligand was used {[M(porph)(bpy)₂]_n (M = CoII, MgII; porph = T pivPP, TPP, TPBP)

[25,33]. Recently, we also reported the preparation of new *meso*-substituted porphyrin [Mg^{II}(TPBP)] (TPBP = *meso*-tetakis[4-(benzoyloxy)phenyl]porphyrin) by combining an ester function comprising two benzene rings with a magnesium(II) atom and two six-coordinate magnesium complexes [Mg(TPBP)(L)₂] (L = HTMA or DABCO) [16]. As the development of ester functions with porphyrins have attracted much attention thanks to their wide range of applications [34,35], it was pointed out that these compounds possess interesting activities against several bacterial species including *Escherichia coli*, *Staphylococcus aureus*, *Bacillus subtilis* and *Pseudomonas aeruginosa*. In this paper, and in continuation of our work on functionalization of *meso* tetra-arylporphyrins, we combined the porphyrin framework Co^{II}(TPBP) with nitrogen based ligand (bpy) to prepare a *hexa*-coordinated 1D linear polymer [Co^{II}(TPBP)(bpy)₂] **1**. Synthesized complex was isolated and structurally characterized by single crystal X-ray diffraction (SCXRD) and natural bond orbital (NBO) computational approach. Physico-chemical properties have been reported based on data from elemental analysis, infrared, proton nuclear magnetic resonance and mass spectrometry, UV–vis absorption and fluorescence spectroscopies. Finally, the antioxidant activity has been determined through scavenging effect on DPPH and ABTS radicals.

2. Materials and methods

2.1. Syntheses and crystallization

Macrocycle of *meso*-tetrakis[4-(benzoyloxy)phenyl]porphyrin (H₂TPBP) was synthesized according to method described in the literature [16,36]. The insertion of cobalt into porphyrin molecule was done by the dimethylformamide method [37,38].

2.1.1. (*meso*-Tetrakis[4-(benzoyloxy)phenyl]porphyrinato)cobalt(II) complex [Co^{II}(TPBP)]

H₂TPBP porphyrin (50 mg, 0.43 mmol) in 150 mL DMF was heated at 150 °C. CoCl₂ (200 mg, 8.6 mmol) was then added and the reaction mixture was stirred until disappearance of the starting material controlled by UV–vis spectroscopy (2 h). After that, the solution was cooled to 50–60 °C and H₂O (50 mL) was added to it. After filtration, the crude product was purified on silica gel column, using a mixture CHCl₃/Hexane (9:1) as eluent, to give after evaporation of a brick red solid. Yield: 60%. ¹H NMR [DMSO-*d*₆, 300 MHz]: δ (ppm) 12.52 (s, 8H, Hβ-pyrrol), 9.23 (d, 8H, *J* = 6.5 Hz), 8.55 (d, 8H, *J* = 8.20 Hz), 7.78 (d, 8H, *J* = 8.7 Hz), 7.67 (m, 12H). UV/vis [λ_{max} (nm) in CH₂Cl₂, (log ε)]: 412 (6.07), 528 (5.58). MS [ESI]: *m/z* calcd for C₇₂H₄₄CoN₄O₈: 1152.0749, found: 1152.1142. Anal. Calcd. for C₇₂H₄₄CoN₄O₈: C; 75.06; H; 3.8; N; 4.8. Found: C; 74.76; H; 3.7; N; 4.94. FTR-IR cm⁻¹: 2964–2853

(νCH porphyrin), 1731 (νC=O ester), 1267 (νC–O ester), 1023 (δCCH porphyrin).

2.1.2. Synthesis of [Co^{II}(TPBP)(bpy)₂] (I)

[Co^{II}(TPBP)] (20 mg, 0.017 mmol) and bpy (90 mg, 0.57 mmol) in 5 mL of dichloromethane (DCM) were stirred overnight at room temperature and the color of the reaction mixture changed from brick red to greenish-orange. Crystals of the desired complex were obtained by slow diffusion of n-hexane through the dichloromethane solution. ¹H NMR [DMSO-*d*₆, 300 MHz]: δ_H (ppm) 13.02 (s, 8H, Hβ-pyrrol), 9.35 (d, 8H, *J* = 6.8 Hz), 8.61 (d, 8H, *J* = 8.60 Hz), 7.88 (d, 8H, *J* = 8.4 Hz), 7.71 (m, 12H), 5.81 (d, 8H-ligand, *J* = 6.4 Hz). UV/vis [λ_{max} (nm) in CH₂Cl₂, (log ε)]: 435 (5.75), 552 (4.49). MS [ESI]: *m/z* calcd for C₈₂H₅₂CoN₆O₈: 1308.3173 [M]⁺, found: 1308.3251. Anal. Calcd. for C₈₄H₅₄Cl₂CoN₆O₈: C; 71.14; H; 3.90; N; 6.03. Found: C; 71.15; H; 4.00; N; 6.91. FTR-IR cm⁻¹: FTR-IR cm⁻¹: 3051 (νCH bpy), 2843 (νCH porphyrin), 1740 (νC=O ester), 1265 (νC–O ester), 1060 (δCCH porphyrin), 800 (δNCH ligand).

2.2. X-ray crystal analysis of complex I

Greenish-orange crystal with approximate dimensions 0.12 mm × 0.25 mm × 0.08 mm was selected for the X-ray diffraction experiment. Data collection was performed on a Bruker APEX-II diffractometer, equipped with graphite monochromated Mo Kα radiation (λ = 0.71073 Å) and intensity data were collected by the narrow frame method at room temperature. The structure was solved by direct method using SIR-2004 [39] and refined by full-matrix least-squares on F2 using the SHELXL-97 program [40] and Data were corrected for absorption effects by the Multi-Scan method [41]. Since the dichloromethane solvent molecule was grossly disordered and could not be modeled, its contribution was excluded using the subroutine SQUEEZE [42].

2.3. Physical and spectroscopic measurements

¹H NMR spectra were recorded on a Bruker AVANCE spectrometer (400 MHz). UV–Vis spectra were measured with a Varian Cary 5000 spectrophotometer. Fluorescence spectra and quantum yield measurements were performed using a Varian Cary Eclipse luminescence spectrophotometer. Elemental analyses were carried out using a Flash EA 1112 Series Thermo Electron fitted with a Porapak column 2 m PTFE + MX5 microbalance Mettler Toledo. The Thermo Scientific “Q Exactive” mass spectrometer was operated under electrospray ionization (ESI) in positive mode with the following settings: accelerating voltage 20 kV, grid voltage 62% of accelerating voltage, extraction delay time of 100 ns.

2.4. Antioxidant studies

The antioxidant activity of the free-base porphyrin H₂TPBP, [Co^{II}(TPBP)] and the [Co^{II}(TPBP)(bpy)₂] complex was evaluated in vitro via their ability to scavenge DPPH and ABTS radicals.

2.4.1. DPPH free radical scavenging assay

The DPPH assay was used for the free radical-scavenging activity of porphyrin compounds. In the experiments, different concentrations of our compounds were taken (prepared in DMSO) and 4.0 mL of DPPH (0.004%) in methanol solution was added to porphyrin compound mixture. After 30 min incubation at room temperature, the absorbance was read against a blank at 517 nm. DPPH radical scavenging activity was calculated using the following formula:

$$\% \text{ Inhibition of DPPH} = \left(A_0 - \frac{A_1}{A_0} \right) \times 100$$

where A₀ was the absorbance of the control and A₁ was the absorbance of the presence of compounds. Vitamin C has been used as standards and their scavenging ability was compared with our results. IC₅₀ (50% inhibition concentration) values of porphyrin compounds and standard (Vitamin C) were also calculated for comparison. IC₅₀ value of the sample is the required concentration to scavenge 50% of DPPH free radicals.

2.4.2. ABTS free radical scavenging assay

The ABTS radical cation (ABTS^{•+}) was produced by reacting ABTS aqueous stock solution (2 mM) with 0.17 mM potassium persulfate and allowing the mixture to stand in the dark at room temperature for 16 h. Before use, this solution was diluted with ethanol to get an absorbance of 0.700 ± 0.020 at 734 nm. Various concentrations (100 μL) of the porphyrin compounds (prepared in DMSO) were added to this solution of ABTS. The absorbance was read against a blank at 734 nm. As for the antiradical activity, ABTS scavenging ability was expressed as IC₅₀ (μg/ml). The inhibition percentage of ABTS radical was calculated using the following formula:

$$\% \text{ Inhibition of ABTS} = \left(A_0 - \frac{A_1}{A_0} \right) \times 100$$

where A₀ is the absorbance of the control, and A₁ is the absorbance of the sample. Vitamin C was used as an appropriate standard.

2.5. Computational details

Density functional theory (DFT) calculations were performed to investigate the natural bond orbital NBO and natural population NPA analyses starting from the experimental single-crystal X-ray structure as input geometry. The Gaussian 09, RevD.01 software package [43], was used for all calculations. The molecular surface plots were visualized by GaussView 6.0 program [44] and The AVOGADRO 1.2.0 molecular viewer [45]. The geometry optimization presented here was accomplished in the gas phase, as a spin unrestricted open-shell system, using Becke's three parameter hybrid exchange and the nonlocal correlation functional of Lee, Yang and Parr (UB3LYP) [46–48]. A quasi-relativistic Stuttgart/Dresden (SDD) effective core potential [49] was used on Co, and 3–21 basis set was used for all other elements. Frequency calculations on optimized geometry ensured that structures were min-

Table 1 Crystal data and structure refinement of complex **1**.

Chemical formula	C ₈₂ H ₅₂ CoN ₆ O ₈
Formula weight	1308.23
Crystal system	monoclinic
Space group	P2/c
<i>a</i> [Å]	17.7767(5)
<i>b</i> [Å]	11.6320(4)
<i>c</i> [Å]	17.9779(6)
α [°]	90
β [°]	115.277(1)
θ [°]	90
<i>V</i> [Å ³]	3361.51(19)
<i>Z</i>	2
<i>D</i> _{calcd.} [g/cm ³]	1.293
μ [mm ⁻¹]	0.319
Max./min. transmission	0.975/0.955
<i>F</i> (0 0 0)	1354
Crystal size [mm]	0.25/0.12/0.08
<i>T</i> (K)	150
Unique data	7691
Unique obsd data	5290
Final <i>R</i> indices	<i>R</i> ₁ = 0.0491, <i>wR</i> ₂ = 0.1453

ima (zero imaginary frequency) on the potential energy surface. On the basis of this optimized molecular geometry, more accurate energies were obtained by performing SP single-point calculations with a larger standard basis set 6-31G(d)/SDD.

3. Results and discussion

3.1. Crystal structure description

The structure of [Co^{II}(TPBP)(bpy)₂] complex was isolated and structurally characterized. Crystallographic data are

summarized in Table 1. The complex crystallizes in the monoclinic system and P2/c space group with *a* = 17.7767(5) Å, *b* = 11.6320(4) Å, *c* = 17.9779(6) Å, β = 115.277(1)°, *V* = 3361.51(19) Å³, *Z* = 2. Selected bond distances and angles are listed in Table S1. In the title Cobalt(II) complex, the asymmetric unit presents one half [Co^{II}(TPBP)(L)] (L = bpy) complex ion and one disordered dichloromethane molecule as solvent. The disordered dichloromethane (DCM) solvent in the lattice was not included in the refinement but was taken care of by the SQUEEZE procedure. A view of the repetitive unit is presented in Fig. 1. The coordination sphere of Co(II) cation is described as distorted octahedron, in which equatorial positions are occupied by four pyrrole nitrogen atoms and the other two come from two N-donor atoms of the bpy molecules (Fig. 2). Structural arrangement along the *a*-axis and the crystal packing are presented in Figs. 3 and 4, respectively. As observed in previously reported polymeric structures [27,28,31,50], our framework consists of 1D polymeric chain extending along the [0 0 1] direction (Fig. 4) where the polymeric moiety maintains so-called “shish kebab” like architectures, in which the cobalt centers are bridged by bpy ligands, forming a linear Co-bpy-Co chain with the Co···Co distance across the bpy ligand equal to 11.675 Å. The Co atom is displaced toward one of two bpy ligands by 0.033 Å. This arrangement is similar to other described assemblies, based on Co^{II}TPP unit, reported by Marijuan et al. [27] and Mansour et al. [28]. The key structural parameters of some characterized polymeric of cobalt(II) porphyrin complexes are given in Table S2. The Co–N_{ax} distances range between 2.265 (2) Å (Co1–N3) and 2.290 (2) Å (Co1–N4) indicating the strong coordination of bpy to metalloporphyrin which seems in agreement with Co–N_{ax} bond length observed in [Co^{II}(porph)L] species with similar axial ligands. In comparison with other polymeric (bpy)-magnesium porphyrin complex, the Mg–N_{ax}(bpy) distances is around ~2.319 Å and 2.290 Å [33]. The bond lengths Co(1)–N(1) and Co(1)–N(2)

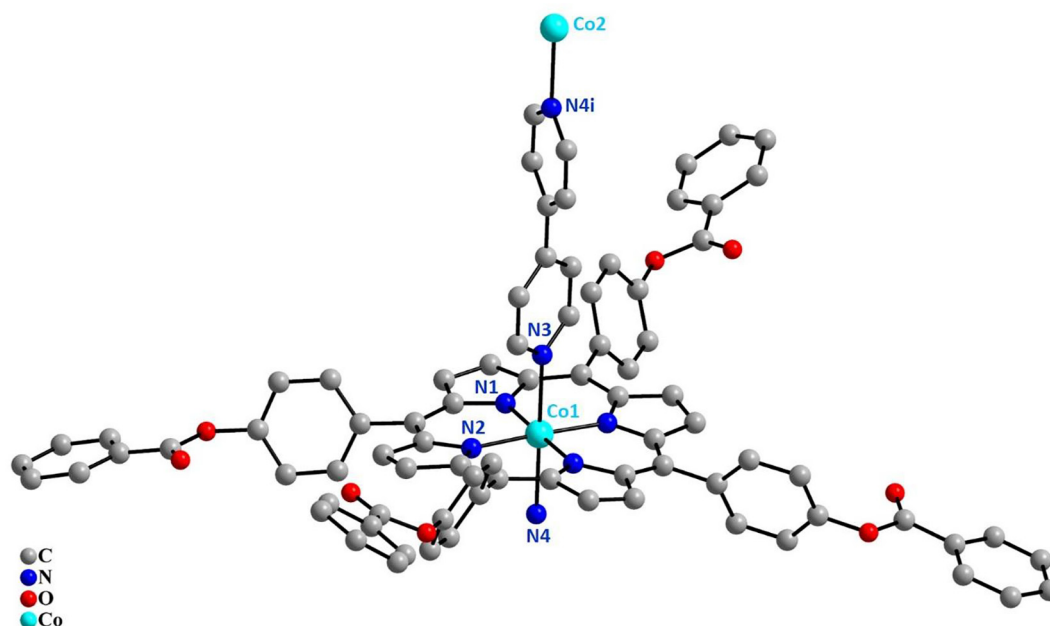


Fig. 1 The building repetitive unit of [Co^{II}(TPBP)(bpy)₂] (**1**) (H atoms are omitted for clarity).

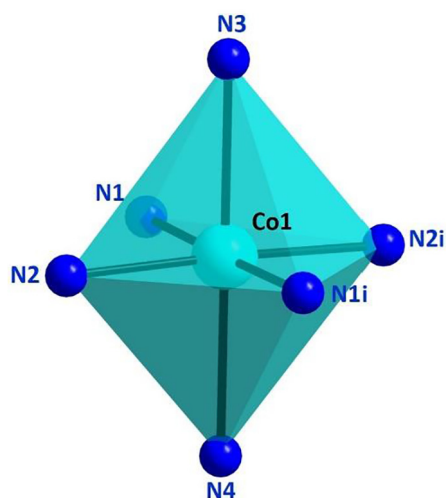


Fig. 2 Coordination geometries around Co1.

are 2.005(2) and 2.155(2) Å, respectively. These bonds are consistent with those found in analogous six-coordinate compounds [28]. The coordination complex assemblies strongly depend on the selection of both metallic centers and bonded ligands [51–53]. Among the multi-dentate N-donor ligands whose coordination behavior has been studied is bpy which is a fairly strong organic base and possesses two potential nitrogen donor atoms. Besides interacting with metal ions, bpy has the capability to form diverse molecular adducts and supramolecular assemblies, due to its good H-bond accepting behavior [54–56]. Here, we report the structure of [Co^{II}(TPBP)(bpy)₂] complex, assembled by bpy in octahedral coordination geometry. The first pyridyl moiety of bpy axial ligand is 25.40°, and the bpy molecule is twisted with dihedral angle 59.05° between the two pyridyl moieties. In general, dihedral angle values in bpy complexes range from 24° to 58° [28,33,57–59]. Interatomic distances and angles describing

CoN₆ octahedron are reported in Table 2. The Co–N distances vary from 1.978 (17) to 2.290 (2) Å with an average value $\langle \text{Co–N} \rangle = 2.134$ Å. The N–N distances vary from 2.787 (20) to 3.044(24) Å with an average value $\langle \text{N–N} \rangle = 3.030$ Å and the angles N–Co–N vary from 88.72 (5) to 91.28 (5)° with an average value $\langle \text{N–Co–N} \rangle = 90.03^\circ$. The calculated distortion indices of angles and distances according to Bohr’s method [60] are depicted in Table 2, giving a measure of the regularity about the CoN₆ coordination environment. These values indicated a pronounced distortion of the Co–N bonds, when compared to N–N distances and N–Co–N angles [DI(Co–N) = 0.063, DI(N–N) = 0.035, DI(N–Co–N) = 0.01]. Distortion of macrocycle for complex 1 has also been analyzed. Fig. 5(a) displays the detailed displacements of each porphyrin core atom (in units of 0.01 Å) from the 24-atom mean planes. According to the four types of distortion shown by Scheidt and Lee [61], the top panel show that porphyrin core of [Co^{II}(TPBP)(bpy)] (1) presents major ruffling (*ruff*) distortion (Fig. 5(b)), which is indicated by the values of the *meso*-carbon atoms above and below the porphyrin mean plane. The crystal structure of 1 mainly contains the crystal packing of hydrogen bonds (C42–H42...N1) and short distances between the carbon atom of 4-formylphenylbenzoate and the bpy ligand (Fig. 6, Table 3).

3.2. NBO–Second-order perturbation theory analysis

The charge delocalization interactions that occur between the Co(II) central ion and surrounding ligand nitrogen atoms have been thoroughly explored by a set of quantum-chemical calculations at the density functional theory level (DFT) (UB3LYP/6-31G(d)/SDD). The Natural population analysis was characteristically carried out to predict the valence electron configurations at the interacted atoms. The NPA-NBO framework is the most suitable approach for atomic this issue, since it is less affected by basis set variation. The existence of both pyrrolic porphyrin (N_{py}) and bpy (N_{bpy}) nitrogen as

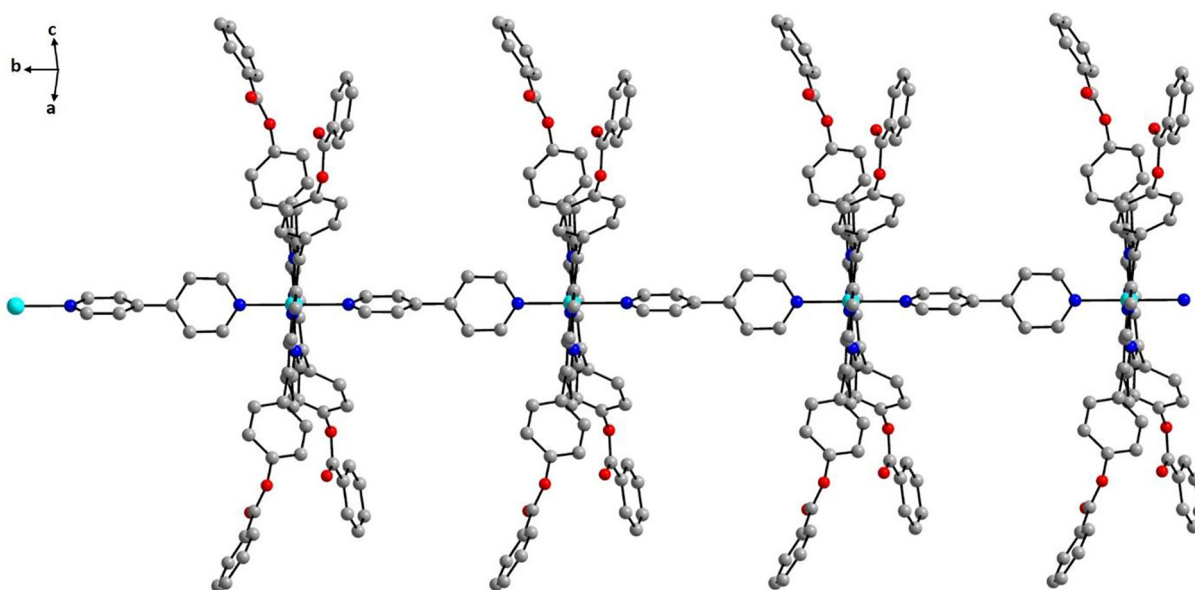


Fig. 3 1D chain linked by the 4,4'-bipyridine ligand.

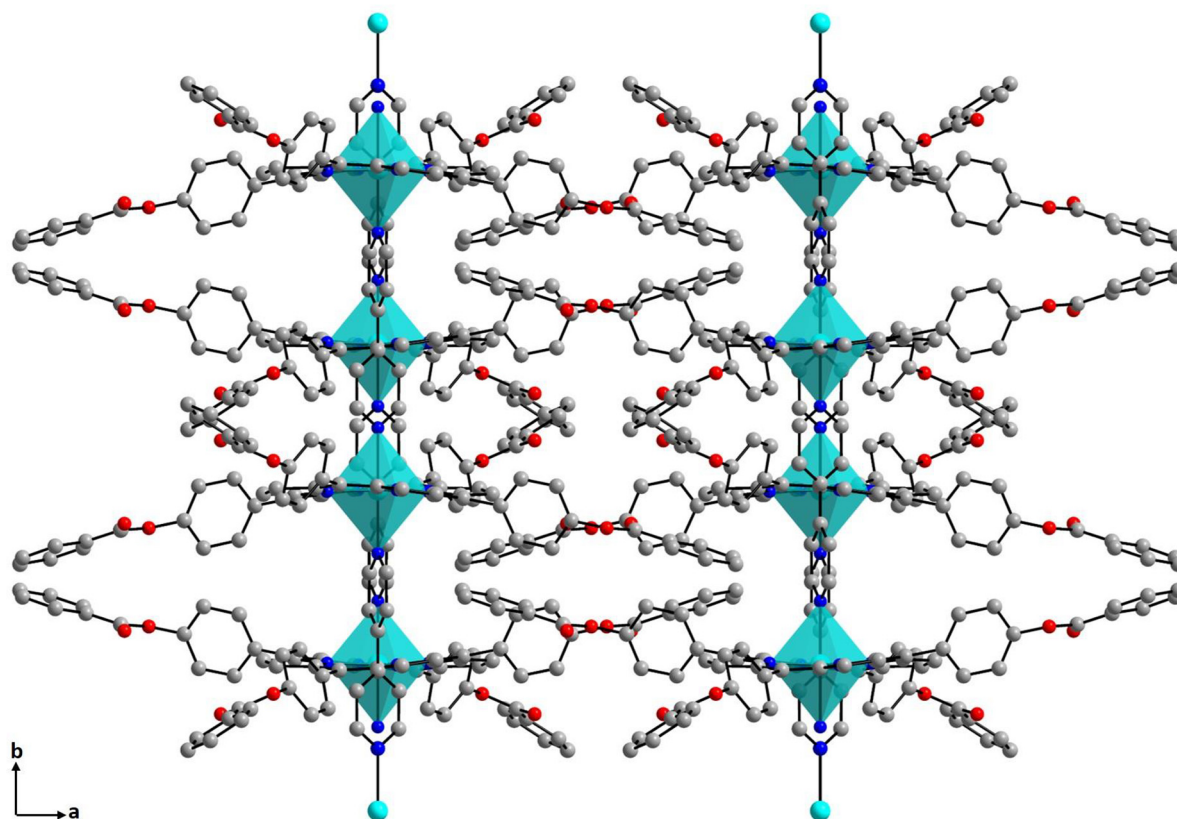


Fig. 4 Projection along the c axis of the atomic arrangement.

Table 2 Bond lengths (Å) and angles (°) in CoN₆ octahedron.

Co	N1	N1i	N2	N2i	N3	N4
N1	<u>1.982 (17)</u>	3.964 (24)	2.816 (32)	2.787 (20)	2.995 (24)	3.044 (24)
N1i	178.87 (9)	<u>1.982 (17)</u>	2.787 (20)	2.816 (32)	2.995 (24)	3.044 (24)
N2	90.60 (7)	89.42 (7)	<u>1.978 (17)</u>	3.957 (29)	3.041 (25)	2.993 (25)
N2i	89.42 (7)	90.60 (7)	177.44 (10)	<u>1.978 (17)</u>	3.041 (25)	2.993 (25)
N3	89.44 (5)	89.44 (5)	91.28 (5)	91.28 (5)	<u>2.265 (2)</u>	4.555 (33)
N4	90.56 (5)	90.56 (5)	88.72 (5)	88.72 (5)	180 (1)	<u>2.290 (2)</u>
<i>DI[Co-N] = 0.063</i>		<i>DI[N-N] = 0.035</i>		<i>DI[N-Co-N] = 0.01</i>		

Bold values indicate distances and angles between diametrically opposed atoms (relative to the cobalt atom).

Bold underline values indicate distances between Co and N atoms.

Italic values indicate distortion indices.

bonded atoms offers an occasion to enrich the inquiry of electron donation tendency. Interestingly, the central cobalt(II) cation has a formal d^7 valence configuration, however investigating the orbital populations we find the following electronic arrangement [core] $4s^{(0.57)}3d^{(7.75)}4p^{(1.21)}4d^{(0.02)}5p^{(0.04)}$ as 17.99878 core electrons, 9.53093 valence electrons and 0.06585 Rydberg electrons. Additionally, all coordinated ligand atoms have a valence electron configuration lower than these expected as [core] $2s^{(1.41)}2p^{(3.70)}$, [core] $2s^{(1.41)}2p^{(3.69)}$, [core] $2s^{(1.46)}2p^{(3.59)}$ and [core] $2s^{(1.45)}2p^{(3.60)}$ for N1, N2, N3 and N4 respectively. These results indicated the transfer of a significant amount of electron density from ligand units to the cobalt(II) center. Therefore, the studied complex could

be described as ligand-to-metal charge-transfer (LMCT) complex since the donations from ligand to metal are higher than the back donation. The Co–N_{py} and Co–N_{bp} interactions were carefully discussed through NBO–Second-order perturbation theory. The second order perturbative energies $E^{(2)}$ corresponding to potential donor–acceptor interactions between ligand donor orbitals (NBO(i)) and metal acceptor orbitals (NBO(j)) are reported in Table 4, the data were selected on accordance of the symmetry. At first sight, we notice that the studied system does not incorporate a bond BD (electron pairs centered on two atoms) between the N_{py}/N_{bp} atoms and the cobalt ions (Co), seeing that the Co–N_{py}/N_{bp} interactions are coming from an electronic delocalization between the

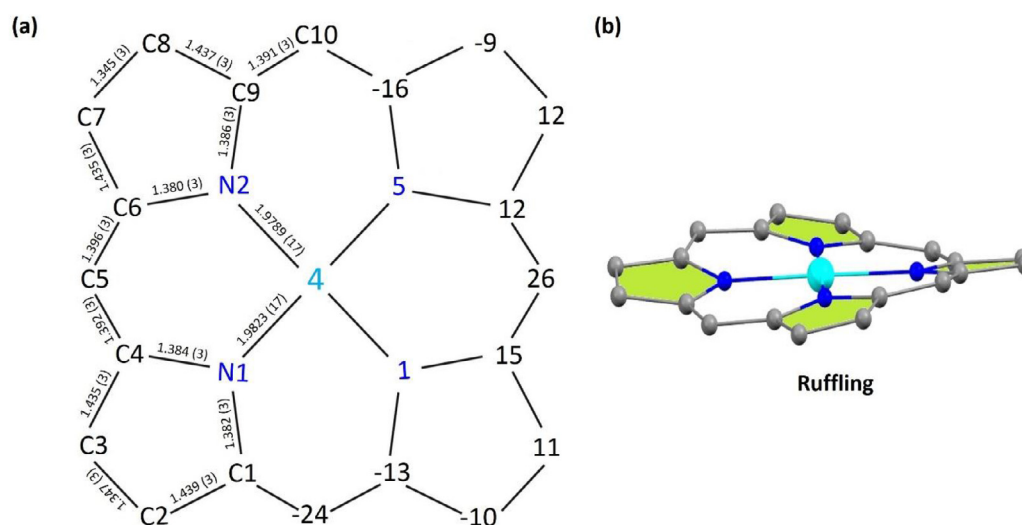


Fig. 5 A diagram of the porphinato core showing, on the upper half, the structurally independent bond lengths and the numbering scheme used throughout this paper for the atoms. On the lower half of the diagram, the numbered symbols for each atom is re-placed by its perpendicular displacement, in units of 0.01 Å, from the mean plane of the porphinato core.

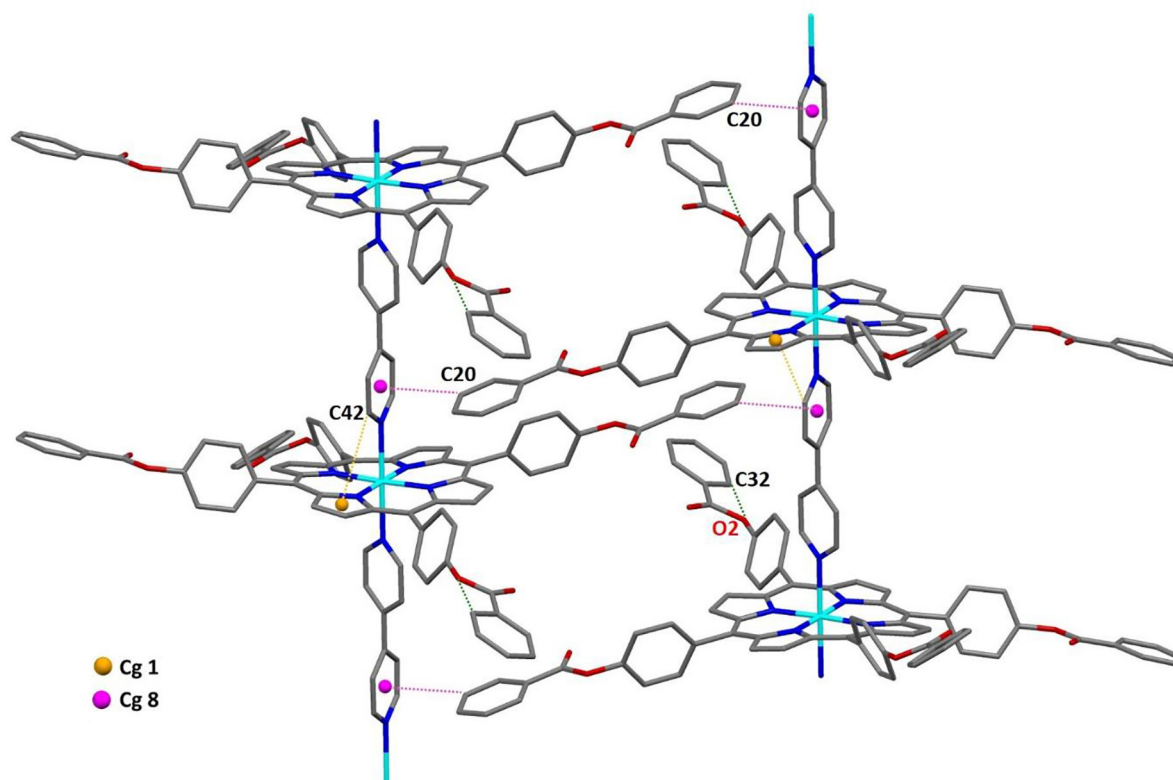


Fig. 6 Schematic representation showing the weak C32–H32···O3 intramolecular hydrogen bond, and the weak C–H···Cg π intermolecular interactions in (1).

N_{py}/N_{bp} filled orbitals to the empty anti-bonding $LP^*(4)$ and $LP^*(5)$ metal orbitals. Visualizations of selected natural orbitals involved in the Co– N_{py} and Co– N_{bp} interactions are given in Figs. 7 and 8. The stabilization energies for $\pi(N1-C4) \rightarrow LP^*(4)Co$ and $\pi(N2-C6) \rightarrow LP^*(4)Co$ are 7.35 and 7.62 kcal/mol, respectively. The lower interaction energies associated

with $\pi^*(N1-C4) \rightarrow LP^*(4)Co$ and $\pi^*(N2-C6) \rightarrow LP^*(4)Co$ are found to be 4.88 and 4.99 kcal/mol, respectively. The larger contribution to the stabilization of coordination system is observed for $LP(N3)/(N4) \rightarrow LP^*(4)/(5)Co$. The net $E^{(2)}$ energies are 78.09 and 77.57 kcal/mol for Co– $N_{bp}(3)$ and Co– $N_{bp}(4)$, respectively (Table 4). Moreover, we found from

Table 3 Inter- and intra-molecular interactions for **1**.

D–H...A	D–H	H...A	D...A	D–H...A
C32–H32...O3 [i]	0.95	2.37	2.705(4)	100
C42–H42...N1 [i]	0.95	2.54	3.128(3)	120
C–H...Cg (π)	H...Cg (π)		C...Cg (π)	C–H...Cg (π)
C20–H20...Cg8 [ii]	2.56		3.482(3)	162
C42–H42...Cg1 [iii]	2.79		3.620(2)	146

A = acceptor, D = donor, X = heteroatom, Cg = centroid.

Cg1: N1/C1–C4 five-member ring, Cg8: is the centroid of the N4/C42a–C42c six-member ring.

Symmetry codes: (i): x, 1 + y, z; (ii): 1 – x, –y, 1 – z; (iii): x, 1 + y, z.

Table 4 The second order perturbative energies $E^{(2)}$ corresponding to donor–acceptor interactions between ligand donor orbitals (NBO(i)) and metal acceptor orbitals (NBO(j)).

Donor NBO(i)	Acceptor NBO(j)	$E^{(2)}$ (kcal/mol)
π (N1–C4)	LP*(4)Co	7.35
π^* (N1–C4)	LP*(4)Co	4.88
π (N2–C6)	LP*(4)Co	7.62
π^* (N2–C6)	LP*(4)Co	4.99
LP(1)N3	LP*(4)Co	49.72
LP(1)N3	LP*(5)Co	28.37
LP(1)N4	LP*(4)Co	44.69
LP(1)N4	LP*(5)Co	32.88

LP: 1-center valence lone pair, *: Antibonding.

the NBO analysis that other kinds of coordinative electronic delocalizations occur although with lower energies, such as LP(1)C9 \rightarrow LP*(5)Co (1.22 Kcal/mol), for σ (C1–C2) \rightarrow σ^* (Co–N1) (1.17 Kcal/mol) and σ (C6–C7) \rightarrow σ^* (Co–N2) (1.23 Kcal/mol).

3.3. ^1H NMR spectroscopies

^1H NMR spectral analysis was carried out at 300 K in DMSO to investigate the structures of our compound. As previously mentioned, the H β -pyrrolic and aromatic protons of the *meso*-phenyl rings of the free porphyrin resonating in the 8.91–7.59 ppm domain (Fig. S1a). [Co^{II}(TPBP)] in DMSO-*d*₆ has paramagnetic properties due to 3d configuration of cobalt

(II), since signals of H β -pyrrolic protons appear as broad singlet at 12.52 ppm, and shifts were also observed of the aromatic protons of the *meso*-phenyl rings in a weak field to 9.23 and 7.67 ppm (Fig. S1b). The ^1H NMR spectrum of [Co^{II}(TPBP)(bpy)₂] (Fig. S1c) indicates that the β -pyrrole protons resonate as a singlet at 13.02 ppm. The aromatic protons of the *meso*-phenyl rings resonate in the 9.35–7.71 ppm range, which are slightly downfield (deshielded) compared to [Co^{II}(TPBP)] compound. The position and sharpness of the ^1H NMR resonances clearly demonstrate the paramagnetic nature of the complex, indicative of a Co(II) complex. The bpy proton signals at 5.81 ppm are shifted upfield from the analogous free pyridine resonances because of the ring current effect, which clearly dictates its axial ligation to the metal center.

3.4. Photophysical properties

3.4.1. UV–vis absorption spectroscopy

The UV–vis spectra of the free-base porphyrin H₂TPBP, [Co^{II}(TPBP)] starting material and complex **1** recorded in dichloromethane are shown in Fig. 9. The λ_{max} values of these species are reported in Table S3 and compared to several other *meso*-porphyrins – cobalt metalloporphyrins. The free-base porphyrin macrocycle H₂TPBP has demonstrated an intense *Soret* or *B* band (corresponding to strongly allowed transition to S₂ state) at 419 nm and four weaker *Q* bands between 515 and 646 nm. The [Co^{II}(TPBP)], exhibits electronic spectra, which is slightly blue shifted compared to this of the free base, with *Soret* and *Q* bands at 412 nm and 528 nm, respectively. The number of *Q* bands decreases from four to a single band

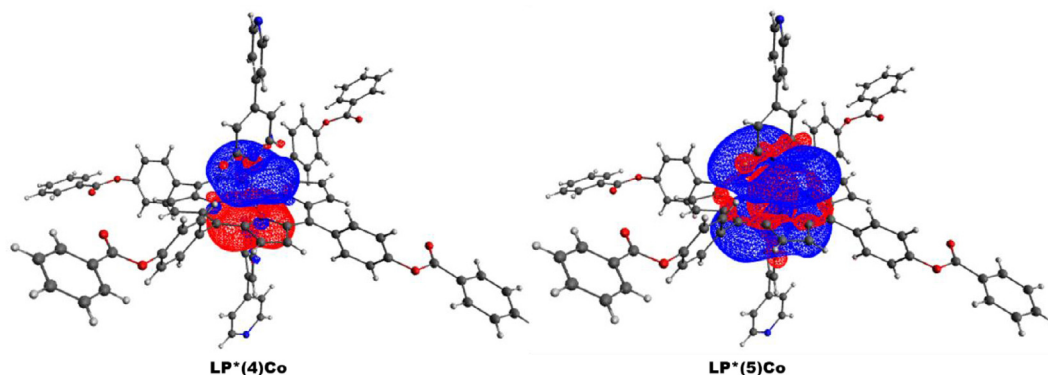


Fig. 7 Visualization of the anti-bonding natural orbitals of Co cation shared in the N_{py}/N_{bp} \rightarrow Co interactions.

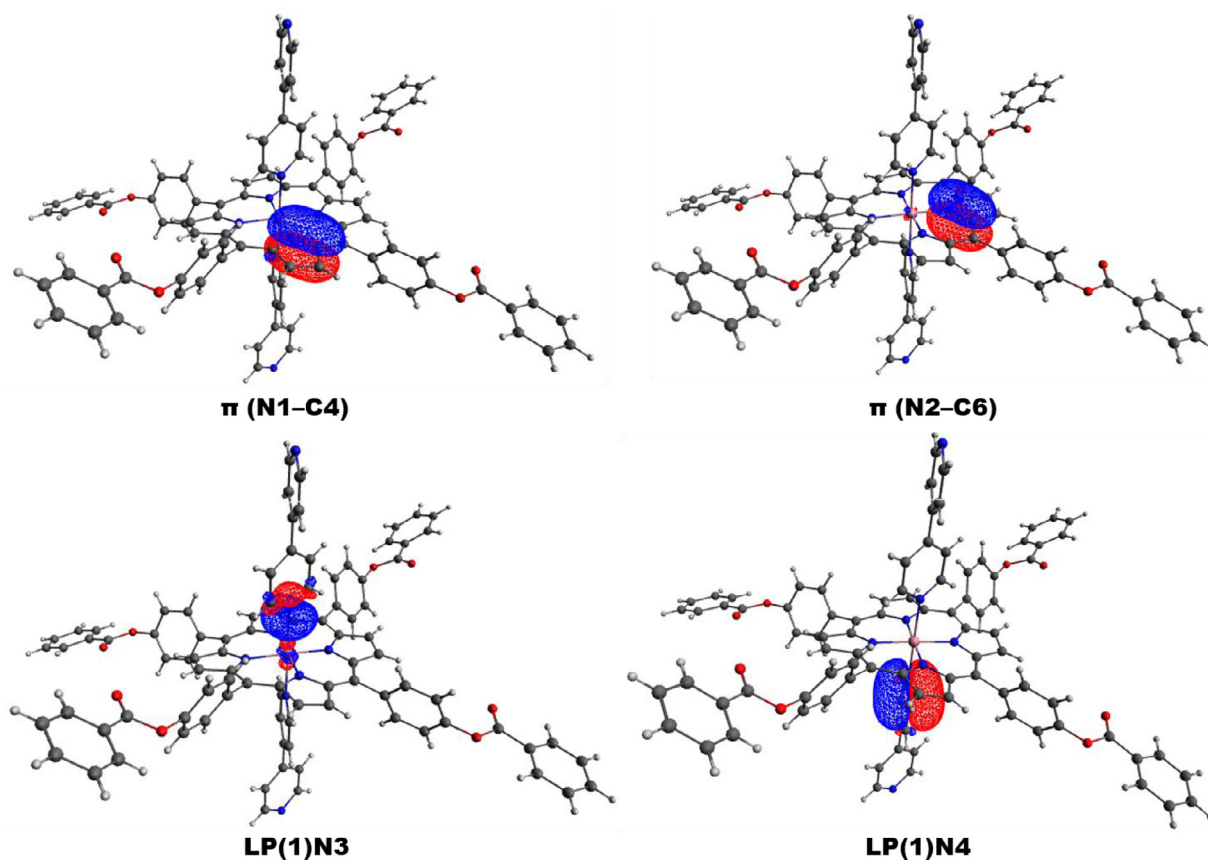


Fig. 8 Visualization of the natural orbitals of the N_{py} and N_{bp} ligand donor atoms shared in the $N_{py}/N_{bp} \rightarrow Co$ interactions.

when going from the free porphyrin to the metalated one, in agreement with the insertion of the cobalt in the porphyrin core. On the other hand, for complex **1** the *Soret* and *Q* bands values are at 435 nm and 552 nm respectively, the *Soret* band is found to red shifted up to 23 nm along with the significant bathochromic shift in their *Q* bands possibly due to an increase in p-conjugation upon addition of bpy ligand. We notice also that the λ_{max} values of the *Soret* and *Q* bands for our cobalt derivative are close to those of the species found in literature [28].

3.4.2. Steady-state emission spectroscopy

The room temperature fluorescence spectra in dichloromethane ($\sim 10^{-6}$ mol L⁻¹) are shown in Fig. 10. The values of the fluorescence quantum yields (Φ_f) of the starting material H₂TBPP, metalloporphyrin [Mg^{II}(TPBP)], and synthesized complex **1** were measured (Table S4). The fluorescence of the B (*Soret*) band is attributed to the transition from the second excited singlet state S₂ to the ground state S₀, S₂ → S₀. The *Soret* fluorescence is about 2 orders of magnitude weaker than that of the S₁ → S₀ transition of the *Q* band emission. When the hydrogen atoms in the center of porphyrin ring are replaced by metal ion, the fluorescence quenching is a well-known phenomenon [62]. From Fig. 10 it can be seen that the free base porphyrin upon excitation at 528 nm displayed two emission peaks S₁ → S₀ centered at 652 nm (S₁ [*Q* (0,0)] → S₀) and 719 nm (S₁ [*Q* (0,1)] → S₀) (Fig. S2a). Similarly, [Co^{II}(TPBP)] displays a main emission band at 653 nm

and a weaker band at 719 nm, upon excitation at 552 nm (Fig. S2b). When excited at 550 nm, [Co^{II}(TBPP)(bpy)₂] complex exhibits two split emission bands at 652 nm (S₁ [*Q* (0,0)] → S₀) and at 718 nm (S₁ [*Q* (0,1)] → S₀) (Fig. S2c). It is noteworthy that the values of λ_{max} of the bands *Q* (0,0) and *Q* (0,1) of the [Co^{II}(TBPP)] ion and complex **1** are practically the same, which is similar to that in the free porphyrin but with a lower intensity. The fluorescence characteristics of cobalt(II) compounds are essentially consistent with those already reported in the literature [63–66]. The accepted interpretation is as follows: (i) the insertion of the cobalt in the porphyrin core has no effect in the position of the *Q* (0,0) and *Q* (0,1) bands, (ii) The fluorescence intensities of cobalt(II) complexes were much weaker than the free porphyrin because cobalt weakened the fluorescence radiation [67]. The fluorescence quantum yields of H₂TPBP, [Co^{II}(TBPP)] and complex **1** are 0.057, 0.032 and 0.036, respectively. These values are lower compared to their corresponding Mg derivatives [16,33]. This could be related to the paramagnetic nature of Co center, which encourages intersystem crossing to the triplet state, hence lowering fluorescence [68].

3.5. Antioxidant activity study

Numerous antioxidant methods and modifications have been proposed to evaluate antioxidant activity and to explain how antioxidant agents work. Among them, the 1,1-diphenyl-2-picrylhydrazyl (DPPH) and 2,2'-Azino-bis(3-ethylbenzothiazol

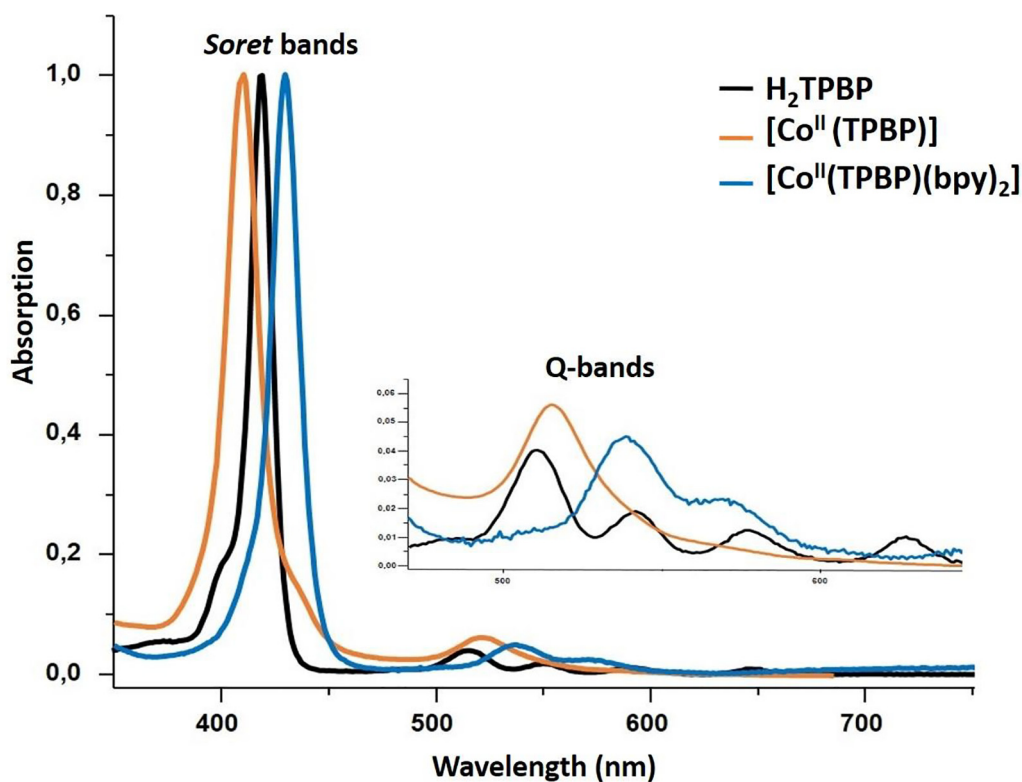


Fig. 9 UV-vis absorption spectra of H_2TPBP , $[\text{Co}^{\text{II}}(\text{TPBP})]$, and $[\text{Co}^{\text{II}}(\text{TPBP})(\text{bpy})_2]$ (**1**), in CH_2Cl_2 solution at concentrations around $10^{-6} \text{ mol L}^{-1}$.

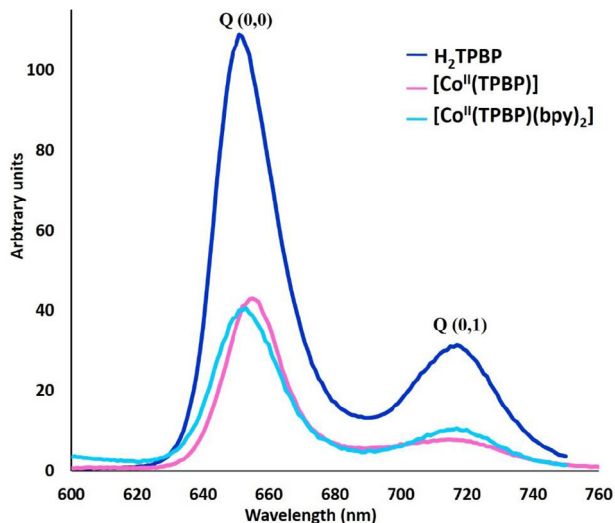


Fig. 10 Emission spectrum of H_2TPBP , $[\text{Co}^{\text{II}}(\text{TPBP})]$, and complex **1** as a $10^{-6} \text{ mol L}^{-1}$ solution in dichloromethane.

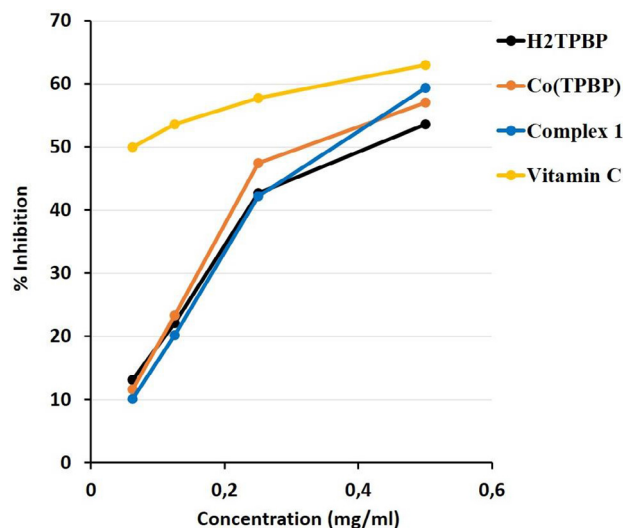


Fig. 11 Radical-scavenging activity on DPPH radicals (%).

line-6-sulfonic acid) (ABTS) radical assays are the most common methods used to determine the radical scavenging ability of various samples. DPPH and ABTS radicals are related with known inflammatory results and have been often used to investigate the potential antioxidant activity of compounds [69] which may bear also a potential anticancer and anti-inflammatory activity [70]. The ability of the free-base porphyrin H_2TPBP , metalloporphyrin $[\text{Co}^{\text{II}}(\text{TPBP})]$ and the

$[\text{Co}^{\text{II}}(\text{TPBP})(\text{bpy})_2]$ (**1**) to scavenge in vitro DPPH, ABTS was evaluated in comparison to the vitamin C reference compound (Figs. 11 and 12, Table 5).

3.5.1. DPPH free radical scavenging activity

In this method, the decolorizing rate of DPPH radical is monitored at a characteristic wavelength in the presence of por-

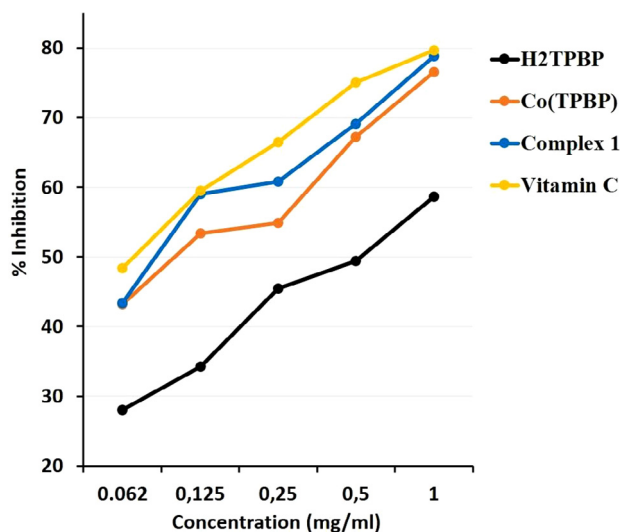


Fig. 12 Radical-scavenging activity on ABTS radicals (%).

Table 5 IC₅₀ values of porphyrin compounds (with and without metal) for DPPH and ABTS scavenging assay. Vitamin c was used as standard.

Compounds/ Standards	IC ₅₀ (mg/mL)	
	DPPH radical scavenging	ABTS radical scavenging
H ₂ TPBP	3.318	2.678
[Co ^{II} (TPBP)]	0.317	0.121
Complex 1	0.364	0.044
Vitamin C	0.0088	0.038

phyrin compounds. In its radical form, DPPH absorbs at 517 nm, but as it is converted to a non-radical form, the color of the solution changes from purple to yellow and this can be observed with a decrease in absorbance [71]. In the present study, the scavenging activities of the free-base porphyrin H₂TPBP, [Co^{II}(TPBP)], the [Co^{II}(TPBP)(bpy)₂] (**1**) complex and standard (vitamin C) against DPPH were evaluated. The percentage antioxidant activity results and IC₅₀ values are given in Fig. 11 and in Table 5 respectively. Various concentrations of the experimental compounds were surveyed.

Studied samples showed radical scavenging activity which increased with increasing of concentrations. For all compounds tested at 1 mg/mL, the highest antioxidant activity was obtained for [Co^{II}(TPBP)] (57.00 ± 0.03%) and [Co^{II}(TPBP)(bpy)₂] (59.00 ± 0.31%) compounds with respect to H₂TPBP free porphyrin (DPPH radical formation inhibition at 0.5 mg/mL). All tested porphyrin compounds showed lower DPPH activity in comparison to standard vitamin C (Fig. 11). As reported in the literature, all the cobalt compounds are more active than the free ligands against DPPH even against other transition metal complexes [72–74], and DPPH radical formation inhibition percent reached 60%. Additionally, IC₅₀ values, defined as the concentration (mg/mL) of compound required for scavenging of DPPH radicals by 50%, were estimated and shown in Table 5. IC₅₀

values were determined by linear regression analysis using at least five different concentrations in duplicate. The higher IC₅₀ values represent lower antioxidant activity. According to the IC₅₀ values, the lowest activity is observed for the free-base porphyrin H₂TPBP (3.318 mg/mL). On the contrary, the Co(TPBP), starting material and the complex **1** shows a high activity, and displayed nearly same IC₅₀ values (0.317 and 0.364 mg/mL respectively), but it's always lower than the standard IC₅₀ values of Vitamin C (0.0088 mg/mL). These results are in line with the fact that the antioxidant activity of the free-base porphyrin increases upon coordination to a metal ion and this increase may be explained by acquisition of an additional radical scavenging metal center by these compounds, which causes an increase in these molecule's ability to stabilize unpaired electrons and therefore to scavenge free radicals.

3.5.2. ABTS free radical scavenging activity

2,2'-Azino-bis(3-ethylbenzothiazoline-6-sulfonic acid) is a moderately stable nitrogen center radical known for its high solubility as compared to the DPPH. ABTS cation is reactive toward most antioxidants including Vitamin C, phenolics, and thiols as well as with any compound that can give a hydrogen atom or an electron. This radical is blue in color and absorbs light at 734 nm. During this reaction, the blue ABTS radical cation is converted back to its colorless neutral form. The ABTS radical scavenging activities of the free-base porphyrin H₂TPBP and its corresponding cobalt compounds, are displayed in Fig. 12 and Table 5. The results were expressed in terms of % inhibition and IC₅₀.

As shown, % inhibition of the ABTS radical activity followed similar pattern as for DPPH assay. The results revealed that all compounds possess an inhibitory effect on ABTS⁺, and the highest antioxidant activity was obtained for [Co^{II}(TPBP)] and [Co^{II}(TPBP)(bpy)₂] complex. Moreover, the values were significantly increased with increasing of concentrations. [Co^{II}(TPBP)] ions showed 43.22 ± 0.24% ABTS radical formation inhibition at 0.06 mg/mL which slightly increased with increasing of concentration to attain 76.60 ± 0.04%. Moreover, complex **1** results 78.79 ± 0.32% ABTS radical formation inhibition, at 1 mg/mL. These compounds exhibit similar antioxidant activity than the standard vitamin C (48.39 ± 0.02% and 79.67 ± 0.12% of inhibition). IC₅₀ values for the free-base porphyrin H₂TPBP, and their cobalt derivatives was determined and compared to that of vitamin C. The results we obtained are the following: 2.678 for H₂TPBP, 0.121 for [Co^{II}(TPBP)], 0.044 for complex **1** and 0.038 for vit c. These compounds inhibited the ABTS activity with an IC₅₀ in the following order: vit c > complex **1** > [Co^{II}(TPBP)] > H₂TPBP. The ABTS radical scavenging of [Co^{II}(TPBP)] and complex **1** are higher than that of the free-base porphyrin H₂TPBP. Moreover, the results obtained against different radicals confirmed that cobalt complexes are more effective to arrest the formation of ABTS radicals than the DPPH radical.

4. Conclusions

In summary, novel cobalt(II) porphyrin compounds, [Co^{II}(TPBP)] and [Co^{II}(TPBP)(bpy)₂] (**1**) have been prepared and characterized. Linear 1D polymeric chain was observed

in the X-ray structure of the six-coordinate complex yielded a so-called “shish kebab” like architecture and the bidentate axial bpy ligand being aligned perpendicularly to the planes of the porphyrin units. The supramolecular arrangement is maintained by C32–H32...O3 intramolecular hydrogen bonds, and weak C42–H42...Cg1 π intermolecular interactions. DFT-NBO analysis confirmed that studied complex could be described as ligand-to-metal charge-transfer (LMCT) complex. Interestingly, second-order perturbation theory analysis indicating that a two-center bond between the N_{py}/N_{bp} atoms and the cobalt ions (Co) was not found, the Co–N_{py}/N_{bp} interactions are coming from an electronic delocalization between the N_{py}/N_{bp} filled orbitals to the empty anti-bonding LP*(4) and LP*(5) metal NBOs. The UV–visible spectrum of **1** exhibits red-shifted *Soret* band compared to the [Co^{II}(TPBP)] and the fluorescence data are practically the same as those of known cobalt porphyrin complexes. The biological studies reveal that synthesized compounds may be classified as antioxidant agents. Indeed, these complexes present a high antioxidant activity with the ABTS assay.

Acknowledgements

The authors thank The Tunisian Ministry of Higher Education and Scientific Research for the financial support.

Appendix A. Supplementary data

Supplementary data to this article can be found online at <https://doi.org/10.1016/j.jscs.2019.03.003>.

References

- [1] Z. Wang, S. Yuan, A. Mason, B. Repogle, D.-J. Liu, L. Yu, Nanoporous porphyrin polymers for gas storage and separation, *Macromolecules* 45 (2012) 7413–7419.
- [2] L. Lvova, A. Paris, M. Mastroianni, G. Pomarico, M. Santonico, G. Pennazza, C. Di Natale, R. Paolesse, A. D’Amico, SWCNTs modified with porphyrin units for chemical sensing applications, *Procedia Eng.* 5 (2010) 1043–1046.
- [3] A.F. Marijuan, G. Barandik, B. Bazán, M.K. Urtiaga, E.S. Larrea, M. Iglesias, L. Lezama, M.I. Arriortua, Heterogeneous catalytic properties of unprecedented μ -O-[Fe(TCPP)]₂ dimers (H₂TCPP = meso-tetra(4-carboxyphenyl)porphyrin): an unusual superhyperfine EPR structure, *Dalton Trans.* 44 (2015) 213–222.
- [4] T. Zhang, W.B. Lin, Metal–organic frameworks for artificial photosynthesis and photocatalysis, *Chem. Soc. Rev.* 43 (2014) 5982–5993.
- [5] I. Beletskaya, V.S. Tyurin, A.Y. Tsivadze, R. Guillard, C. Stern, Supramolecular chemistry of metalloporphyrins, *Chem. Rev.* 109 (2009) 1659–1713.
- [6] M.J. Crossley, P.L. Burn, An approach to porphyrin-based molecular wires: synthesis of a bis(porphyrin)tetraone and its conversion to a linearly conjugated tetrakisporphyrin system, *J. Chem. Soc., Chem. Commun.* (1991) 1569–1571.
- [7] R. Paolesse, S. Nardis, D. Monti, M. Stefanelli, C.D. Natale, Porphyrinoids for chemical sensor applications, *Chem. Rev.* 117 (2017) 2517–2583.
- [8] D. Khusunudinova, A.M. Beiler, B.L. Wadsworth, S.I. Jacob, G. F. Moore, Metalloporphyrin-modified semiconductors for solar fuel production, *Chem. Sci.* 8 (2017) 253–259.
- [9] T. Nakamura, M. Fujitsuka, Y. Araki, O. Ito, J. Ikemoto, K. Takimiya, Y. Aso, Tetsuo Otsubo, Photoinduced electron transfer in porphyrin-oligothiophene-fullerene linked triads by excitation of a porphyrin moiety, *J. Phys. Chem. B* 108 (2004) 10700–10710.
- [10] S. Isoda, S. Nishikawa, S. Ueyama, Y. Hanazato, H. Kawakubo, M. Maeda, Photo-induced electron transfer in molecular heterojunctions using flavin-porphyrin Langmuir-Blodgett multilayers, *Thin Solid Films* 210 (1992) 290–292.
- [11] C.W. Lee, H.P. Lu, C.M. Lan, Y.L. Huang, Y.R. Liang, W.N. Yen, Y.C. Liu, Y.S. Lin, E.W.G. Diao, C.Y. Yeh, Novel zinc porphyrin sensitizers for dye-sensitized solar cells: synthesis and spectral, electrochemical, and photovoltaic properties, *Chem. Eur. J.* 15 (2009) 1403–1412.
- [12] P. Le Maux, H.F. Srouf, G. Simonneaux, Enantioselective water-soluble ironporphyrin-catalyzed epoxidation with aqueous hydrogen peroxide and hydroxylation with iodobenzene diacetate, *Tetrahedron* 68 (2012) 5824–5828.
- [13] A.N. Vzorov, D.W. Dixon, J.S. Trommel, L.G. Marzilli, R.W. Compans, Inactivation of human immunodeficiency virus type 1 by porphyrins, *Antimicrob. Agents Chemother.* 46 (2002) 3917–3925.
- [14] V. Car, O. Gaud, I. Sylvain, O. Bourdon, M. Spiro, J. Blais, R. Granet, P. Krausz, M. Guilloton, Fungicidal properties of meso-aryl glycosylporphyrins: influence of sugar substituents on photoinduced damage in the yeast *Saccharomyces cerevisiae*, *J. Photochem. Photobiol. B: Biol.* 48 (1999) 57–62.
- [15] K.G. Yu, D.H. Li, Ch.H. Zhou, J.L. Diao, Study on the synthesis and antimicrobial activity of novel cationic porphyrins, *Chin. Chem. Lett.* 20 (2009) 411–419.
- [16] N. Amiri, M. Hajji, F.B. Taheur, S. Chevreux, T. Roisnel, G. Lemercier, H. Nasri, Two novel magnesium(II) tetraporphyrin-based coordination complexes: syntheses, combined experimental and theoretical structures elucidation, spectroscopy, photophysical properties and antibacterial activity, *J. Solid State Chem.* 258 (2018) 477–484.
- [17] G.D. Bajju, V. Kumar, Ashu, Synthesis, comparative studies on the characterisation and biological activity of chlorochromium (III) and chloro-oxo-chromium(V) porphyrins, *World J. Pharm. Res.* 4 (2015) 2148–2170.
- [18] A. Policard, A. Leuller, Etude Sur les aspects offerts par les tumeurs expérimentales examinées à la lumière de wood, *Compt. Rend. Soc. Wood* 91 (1924) 1423–1424.
- [19] F. Megnin, P.J. FaustinoLyon, R.C. Lelkes, P.I. Cohen, Studies on the mechanism of selective retention of porphyrins and metalloporphyrins by cancer cells, *Biochem. Biophys. Acta* 929 (1987) 173–181.
- [20] S. Nakajima, T. Takemura, I. Sakata, Tumor-localizing activity of porphyrin and its affinity to LDL, transferrin, *Cancer Lett.* 92 (1995) 113–118.
- [21] B.B. Wang, H. Zuo, J. Mack, P. Majumdar, T. Nyokong, K.S. Chan, Z. Shen, Optical properties and electronic structures of axially-ligated group 9 porphyrins, *J. Porphyrins Phthalocyanines* 19 (2015) 973–982.
- [22] M.A. Fodor, O. Horváth, L. Fodor, G. Grampp, A. Wankmüller, Photophysical and photocatalytic behavior of cobalt(III) 5,10,15,20-tetrakis(1-methylpyridinium-4-yl)porphyrin, *Inorg. Chem. Commun.* 50 (2014) 110–112.
- [23] R.G. Little, J.A. Ibers, Stereochemistry of cobalt porphyrins. III. The structure of 2,3,7,8,12,13,17,18-octaethylporphyrinato(1-methylimidazole)- cobalt(II). A model for deoxycoboglobin, *J. Am. Chem. Soc.* 96 (1974).
- [24] J.S. Summers, J.L. Petersen, A.M. Stohenberg, Comparison of the structures of the five-coordinate cobalt(II) pyridine, five-coordinate cobalt(III) methyl, and six-coordinate cobalt(III) methyl pyridine complexes of actaethylporphyrin, *J. Am. Chem. Soc.* 116 (1994) 7189–7195.

- [25] W.R. Scheidt, Stereochemistry of Low-Spin Cobalt Porphyrins. III. The crystal structure and molecular stereochemistry of bis(piperidine)- $\alpha,\beta,\gamma,\delta$ -tetraphenylporphinato cobalt(II), *J. Am. Chem. Soc.* 96 (1974).
- [26] Y. Terazono, B.O. Patrick, D.H. Dolphin, X-ray crystal structure and ligand binding to β -tetrakis (trifluoromethyl)-meso-tetraphenylporphyrin cobalt(II), *Inorg. Chim. Acta* 346 (2003) 265–269.
- [27] A.F. Marijuan, G. Barandika, Begoña Bazán, M.K. Urriaga, M. I. Arriortua, Thermal stability and crystallochemical analysis for CoII-based coordination polymers with TPP and TPPS porphyrins, *CrystEngComm* 15 (2013) 4181–4188.
- [28] A. Mansour, Y. Belghith, M.S. Belkhiria, A. Bujacz, V. Guérineau, H. Nasri, Synthesis, crystal structures and spectroscopic characterization of Co(II) bis(4,4'-bipyridine) with meso-porphyrins $\alpha,\beta,\alpha,\beta$ -tetrakis(o-pivalamidophenyl) porphyrin ($\alpha,\beta,\alpha,\beta$ -TpvPP) and tetraphenylporphyrin (TPP), *J. Porphyrins Phthalocyanines* 17 (2013) 1094–1103.
- [29] X. Li, Y. Cheng, J. Mu, Preparation of a new composite consisted of titanate nanotubes and porphyrin oligomer by a capillary filling, *Colloids Surf., A: Physicochem Eng. Aspects* 348 (2009) 24–27.
- [30] R.K. Kumar, Y.D. Posner, I. Goldberg, Solid-state supramolecular chemistry of porphyrins. ligand-bridged tetraphenylmetalloporphyrin dimers, *J. Incl. Phenom. Macrocyclic Chem.* 37 (2000) 219–230.
- [31] S. Dey, S.A. Ikbāl, S.P. Rath, Self-assembly of cobalt(II) and zinc(II) tetranitrooctaethylporphyrin via bidentate axial ligands: synthesis, structure, surface morphology and effect of axial coordination, *New J. Chem.* 38 (2014) 1458–1470.
- [32] X. Li, L. Zhang, J. Mu, J. Qiu, Fabrication and properties of porphyrin nano- and microparticles with novel morphology, *Nanoscale Res Lett* 3 (2008) 169–178.
- [33] N. Amiri, M. Hajji, T. Roisnel, G. Simonneaux, H. Nasri, Synthesis, molecular structure, photophysical properties and spectroscopic characterization of new 1D-magnesium(II) porphyrin-based coordination polymer, *Res. Chem. Intermed.* 44 (2018) 5583–5595.
- [34] D.M. Carminati, D. Intriери, S.L. Gac, T. Roisnel, B. Boitrel, L. Toma, L. Legnani, E. Galloa, Synthesis, characterisation and catalytic use of iron porphyrin amino ester conjugates, *New J. Chem.* 41 (2017) 5950–5959.
- [35] M.F. Isaac, S.B. Kahl, Synthesis of ether- and carbon-linked polycarboranyl porphyrin dimers for cancer therapies, *J. Organomet. Chem.* 680 (2003) 232–243.
- [36] A.D. Adler, F.R. Longo, J.D. Finarelli, J. Goldmacher, J. Assour, L. Korsakoff, A simplified synthesis for meso-tetraphenylporphyrin, *J. Org. Chem.* 32 (1967), 476–476.
- [37] A.D. Adler, F.R. Longo, F. Kampas, J. Kim, On the preparation of metalloporphyrins, *J. Inorg. Nucl. Chem.* 32 (1970) 2445–2448.
- [38] C.A. Pessoa, Y. Gushikem, Cobalt porphyrins immobilized on niobium(V) oxide grafted on a silica gel surface: study of the catalytic reduction of dissolved dioxygen, *J. Porphyrins Phthalocyanines* 5 (2001) 537–544.
- [39] M.C. Burla, R. Caliandro, M. Camalli, B. Carrozzini, G.L. Casciarano, L. De Caro, C. Giacovazzo, G. Polidori, R. Spagna, SIR2004: an improved tool for crystal structure determination and refinement, *J. Appl. Cryst.* 38 (2005) 381–388.
- [40] G.M. Sheldrick, A short history of SHELX, *Acta Crystallogr. A* 64 (2008) 112–122.
- [41] P.J. Becker, P. Coppens, Extinction within the limit of validity of the Darwin transfer equations. I. General formalism for primary and secondary extinction and their applications to spherical crystals, *Acta Crystallogr. A* 30 (1974) 129–147.
- [42] A.L. Spek, Structure validation in chemical crystallography, *Acta Crystallogr. D* 65 (2009) 148–155.
- [43] M.J. Frisch, G.W. Trucks, H.B. Schlegel, Lee, et al, Gaussian 09, Revision D.01, Gaussian Inc, Wallingford CT, 2013.
- [44] R. Dennington, T. Keith, J. Millam, GaussView, Version 6, Semichem Inc., Shawnee Mission, KS, 2016.
- [45] M.D. Hanwell, D.E. Curtis, D.C. Lonié, T. Vandermeersch, E. Zurek, G.R. Hutchison, Avogadro: an advanced semantic chemical editor, visualization, and analysis platform, *J. Cheminform.* 4 (2012) 17, <https://doi.org/10.1186/1758-2946-4-17>.
- [46] C.T. Lee, W.T. Yang, R.G. Parr, Development of the Colic-Salvetti correlation-energy formula into a functional of the electron density, *Phys. Rev B.* 37 (1988) 785.
- [47] R.G. Parr, W. Yang, Density Functional Theory of Atoms and Molecules, Oxford University Press, New York, 1989.
- [48] A.D. Becke, Density-functional thermochemistry. III. The role of exact exchange, *J. Chem. Phys.* 98 (1993) 5648.
- [49] M. Dolg, U. Wedig, H. Stoll, H. Preuss, Energy-adjusted ab initio pseudopotentials for the first row transition elements, *J. Chem. Phys.* 86 (1987) 866.
- [50] S.A. Ikbāl, S. Brahma, S.P. Rath, Building-up remarkably stable magnesium porphyrin polymers self-assembled via bidentate axial ligands: synthesis, structure, surface morphology, and effect of bridging ligands, *Inorg. Chem.* 51 (2012) 9666–9676.
- [51] S.R. Baten, B.F. Hoskins, R. Robson, Two interpenetrating 3D networks which generate spacious sealed-off compartments enclosing of the order of 20 solvent molecules in the structures of Zn(CN)(NO₃)(tpt)₂/3.cntdot.solv (tpt = 2,4,6-tri(4-pyridyl)-1,3,5-triazine, solv = appr.3/4C₂H₂Cl₄.cntdot.3/4CH₃OH or .appr.3/2CHCl₃.cntdot.1/3CH₃OH), *J. Am. Chem. Soc.* 117 (1995) 5385–5386.
- [52] B.F. Hoskins, R. Robson, Design and construction of a new class of scaffolding-like materials comprising infinite polymeric frameworks of 3D-linked molecular rods. A reappraisal of the zinc cyanide and cadmium cyanide structures and the synthesis and structure of the diamond-related frameworks [N(CH₃)₄][CuI₂ZnII(CN)₄] and CuI[4,4',4'',4'''-tetracyanotetraphenylmethane]BF₄.x₆H₅NO₂, *J. Am. Chem. Soc.* 112 (1990) 1546.
- [53] G.B. Gardner, D. Venkataraman, J.S. Moore, S. Lee, *Nature* 374 (1995) 792–795.
- [54] R.F. Klevtsova, L.A. Glinskaya, E.I. Berus, S.V. Larionov, Monodentate and bridging bidentate functions of 4,4'-bipyridine in the crystal structures of [Zn(4,4'-Bipy){(n-C₃H₇)₂NCS₂}]₂ and [Zn₂(4,4'-Bipy){(n-C₃H₇)₂NCS₂}]₄, *J. Struct. Chem.* 42 (2001) 639–647.
- [55] Y.B. Dong, M.D. Smith, R.C. Layland, H.C.Z. Loye, Novel hydrogen-bonded two- and three-dimensional networks generated from the reaction of metal nitrate hydrates (M = Cd, Co) with the bidentate linear ligand 4,4'-bipyridine, *J. Chem. Soc., Dalton Trans.* (2000) 775–780.
- [56] L.P. Zhang, L.G. Zhu, Monodentate function of the 4,4'-bipyridine that systematically occurs in the 4-sulfobenzoate manganese(II) complexes: syntheses, crystal structures, and properties, *CrystEngComm* 8 (2006) 815–826.
- [57] A. Mansour, M. Zaied, I. Ali, S. Soliman, M. Othmani, Synthesis, molecular structure, spectroscopic characterization and antibacterial activity of the Co(III) (chlorido)(pyridine) and (chlorido)(4,4'-bipyridine) “picket fence” porphyrin complexes, *Polyhedron* 127 (2017) 496–504.
- [58] A.D. Shukla, P.C. Dave, E. Suresh, A. Das, P. Dastidar, Multicomponent Zn-tetraphenylporphyrins: syntheses, characterization and their self assembly in the solid state, *J. Chem. Soc., Dalton Trans* (2000) 4459–4463.
- [59] A.F. Marijuan, G. Barandika, B. Bazan, M.K. Urriaga, L. Lezama, M.I. Arriortua, Fe-TPP Coordination network with metalloporphyrinic neutral radicals and face-to-face and edge-to-face π - π stacking, *Inorg. Chem.* 52 (2013) 8074–8081.

- [60] W.H. Baur, The geometry of polyhedral distortions. Predictive relationships for the phosphate group, *Acta Crystallogr. B* 30 (1974) 1195–1215.
- [61] W.R. Scheidt, Y. Lee, Recent advances in the stereochemistry of metallotetrapyrroles, *Struct. Bonding* 64 (1987) 1–70.
- [62] X.M. Guo, T.S. Shi, Preparation and characterization of the self-aggregated dimer of meso-p-hydroxyphenylporphyrin and studies on the self-aggregate reaction mechanism, *J. Mol. Struct.* 789 (2006) 8–17.
- [63] B. Yan, X. Liu, T. Ghugare, N. Fedorka, Y.F. Li, 2D Metalloporphyrin coordination network of cobalt meso-tetra (4-carboxyphenyl)porphyrin, *J. Coord. Chem.* 68 (2015) 2827–2834.
- [64] W. Chen, S. Fukuzumi, Change in supramolecular networks through in situ esterification of porphyrins, *Eur. J. Inorg. Chem.* (2009) 5494–5505.
- [65] Y.X. Du, Z.Q. Zhang, Y.H. Yao, J. Li, Synthesis, structures and properties of a meso-substituted pyrazolyl porphyrin and its Co (II) porphyrin complex, *Inorg. Chem. Commun.* 64 (2016) 19–22.
- [66] J. Patwari, A. Chatterjee, S. Sardar, P. Lemmens, S.K. Pal, Ultrafast dynamics in co-sensitized photocatalysts under visible and NIR light irradiation, *Phys. Chem. Chem. Phys.* 20 (2018) 10418–10429.
- [67] X. Guo, B. Guo, T. Shi, The photochemical and electrochemical properties of chiral porphyrin dimer and self-aggregate nanorods of cobalt(II) porphyrin dimer, *Inorg. Chim. Acta* 363 (2010) 317–323.
- [68] J.R. Darwent, P. Douglas, A. Harriman, G. Porter, M.C. Richoux, Metal phthalocyanines and porphyrin for reduction of water to hydrogen, *Coord. Chem. Rev.* 44 (1982) 83–126.
- [69] C. Kontogiorgis, D. Hadjipavlou-Litina, Biological evaluation of several coumarin derivatives designed as possible anti-inflammatory/antioxidant agents, *J. Enzyme Inhib. Med. Chem.* 18 (2003) 63–69.
- [70] R. Cini, G. Giorgi, A. Cinquantini, C. Rossi, M. Sabat, Metal complexes of the antiinflammatory drug piroxicam, *Inorg. Chem.* 29 (1990) 5197–5200.
- [71] H. Jaberiana, K. Piri, J. Nazari, Phytochemical composition and in vitro antimicrobial and antioxidant activities of some medicinal plants, *Food Chem.* 136 (2013) 237–244.
- [72] M. Aydın, E.H. Alici, A.T. Bilgiçli, M.N. Yarasir, G. Arabaci, Synthesis, characterization, aggregation, fluorescence and antioxidant properties of bearing (4-(methylthio)phenylthio) tetra substituted phthalocyanines, *Inorg. Chim. Acta* 464 (2017) 1–10.
- [73] N. Söylemez, E. Yabaş, S.Ş. Bölükbas, M. Sülü, Antioxidant activities of the new tetrasubstituted metal-free, Zn(II) and Co (II) monophthalocyanines, *J. Porphyrins Phthalocyanines* 22 (2018) 1–10.
- [74] N. Yıldırım, A.T. Bilgiçli, E.H. Alici, G. Arabacı, M.N. Yarasır, Formation, characterization, aggregation, fluorescence and antioxidant properties of novel tetrasubstituted metal-free and metallophthalocyanines bearing (4-(methylthio)phenoxy) moieties, *J. Mol. Struct.* 1144 (2017) 66–79.